



# Boolean and fuzzy logic operators and multivariate linear regression applied to airborne gamma-ray spectrometry data for regolith mapping in granite-greenstone terrain in Midwest Brazil



Sanclever Freire Peixoto<sup>a,b,\*</sup>, Adriana Maria Coimbra Horbe<sup>a</sup>, Túlio Marques Soares<sup>a</sup>, Caroline Araújo Freitas<sup>a</sup>, Endel Muller Dalat de Sousa<sup>a</sup>, Edgar Romeo Herrera de Figueiredo Iza<sup>c</sup>

<sup>a</sup> Universidade de Brasília, Instituto de Geociências, Campus Universitário Darcy Ribeiro, Distrito Federal, Brasília, 70910-900, Brazil

<sup>b</sup> Instituto Natureza do Tocantins-NATURATINS, Q. 302, Norte Alameda 1, s/n - Lote 3, Plano Diretor Norte, Palmas, TO, 77006-336, Brazil

<sup>c</sup> Serviço Geológico do Brasil-CPRM, Salvador, Brazil

## ARTICLE INFO

### Keywords:

Ferruginous and manganese lateritic duricrusts  
Fuzzy logic  
Boolean logic  
Multivariate linear regression  
Map algebra  
Weathering intensity index

## ABSTRACT

Recent studies have proposed several possibilities of combining K, Th and U airborne gamma-ray spectrometry channels to generate predictive algorithms maps. These algorithms can be used for mapping regolith in deeply weathered terrains with residual, erosion, and deposition surfaces helping to developed strategies to better understand the regolith landscape and to improve geomorphology interpretation, and to identify mineral exploration target sites for primary (bedrock or saprolite) or supergene (hosted in lateritic duricrust) ore deposits. With the goal to easily map the regolith, two mathematical procedures were used on airborne gamma-ray spectrometry data in GIS software, validated by fieldwork on granite-greenstone belts in Midwest Brazil: 1. airborne gamma-ray spectrometry and altimetric data integrated in Boolean and fuzzy logic allowed segregating the areas with ferruginous and manganese residual lateritic duricrusts from erosional surface with rocks and saprolite with 90% of accuracy ( $\kappa_{\text{Boolean}} = 0.69$  and  $\kappa_{\text{FAPo}} = 0.66$ ) and 2. airborne gamma-ray spectrometry and altimetric data integrated with weathering stages in multivariate linear regression (basic statistic) helped establish the regional weathering intensity index, with acceptable error ( $r^2 \text{ adjusted} > 0.6$  and  $p\text{-value} < 5\%$ ). These two modeling techniques provide useful, accurate, rapidly and complementary regolith maps and can be applied in large regions for preliminary interpretations.

## 1. Introduction

Deeply weathered regolith occurs mainly in the modern intertropical zone, where strong chemical weathering favors rock transformation, giving rise to stable products in a superficial environment (Costa, 1997; Horbe and Costa, 1999; Anand and Paine, 2002; Freyssinet et al., 2005; Yang et al., 2009; Anand and Butt, 2010). Predictive mapping tools comprise a set of data processing techniques used in GIScience, which can be a “simple” overlay of data layers or an advanced coordinated multiple view environment data layers with complex models on a desktop (Carranza, 2011; Ormeling and Kraak, 2008). Predictive mapping tools can be easily tested and applied to large regions, based on their characteristics such as the density of vegetation cover, humidity, and the extent of anthropization by agriculture and livestock, thereby

helping develop strategies for accurate and rapid regolith exploration.

Supergene gold was found in lateritic duricrusts and mottled horizons in most deposits in the savanna environments of Africa, India, and Brazil (Freyssinet et al., 1989; Santosh et al., 1990; Bowell et al., 1996; Porto and Hale, 1996; Larizatti et al., 2008). For effective greenfield mineral exploration, regolith mapping using integrating mineralogical and geochemical data (e.g., Davy and El-Ansary, 1986; Anand and Paine, 2002; Barnes et al., 2014; Iza et al., 2018) is necessary, especially in a deeply weathered terrain where the overburdens mask paleo residual surfaces and the geochemical redistribution due to weathering forms extensive geochemical anomalies larger than the ore deposit itself (Anand, 2001). Maps showing the distribution of landform-regolith units provide relevant and sometimes subtle information of these terrains, help target selection, and may help in interpreting soil

\* Corresponding author. Universidade de Brasília, Instituto de Geociências, Campus Universitário Darcy Ribeiro, Distrito Federal, Brasília, 70910-900, Brazil.  
E-mail address: [sanclever@yahoo.com.br](mailto:sanclever@yahoo.com.br) (S.F. Peixoto).

geochemical anomalies and identifying supergene mineralization (Smith et al., 2000).

Potassium (K) occurs mainly in primary rock-forming minerals, such as K-feldspar and micas. It is present in high concentrations in felsic rocks (granites, etc.) and low concentrations in mafic rocks. Thorium (Th) and uranium (U) are found as traces in primary rock-forming minerals (e.g., feldspars), but are common in accessory and resistate minerals (zircons, monazite, and xenotime). Th and U occur in high concentrations in granites and K is scarce in mafic rocks (O'Reilly et al., 1988; Dickson and Scott, 1997). The gamma-response reflects the mineralogy and geochemistry of the parent rock, and weathering products, including lateritic duricrusts, mottled horizons, residual and transported clay, sand and gravel (Wilford et al., 1997). Different techniques for the analysis of airborne gamma-ray spectrometry data have been proposed ranging from the ratios of the radiometric channels (Dickson and Scott, 1997; Wilford et al., 1997), agglomerative hierarchical clustering (Martelet et al., 2006), Boolean and fuzzy logic operators (Porwal et al., 2015; Iza et al., 2016), multivariate linear regression (Wilford, 2012; Martelet et al., 2013), artificial neural network classification (Metelka et al., 2018), to combination with optical remote sensing datasets (Voll et al., 2020). Integrated interpretation of airborne gamma-ray spectrometry and Shuttle Radar Topography Mission (SRTM) images has been used to identify geophysical patterns of extensive regolith cover (Dauth, 1997; Jayawardhana and Sheard, 2000;

Wilford et al., 1997; Dent et al., 2013; Arhin et al., 2015; Grimaud et al., 2015; Moonjun et al., 2017; Albuquerque et al., 2020). The successful combination of gamma-ray spectrometry and altimetric data in the regolith mapping is because of the capacity of residual lateritic duricrust to concentrate Th, U, and other trace elements on both Fe oxi-hydroxides and residual minerals (zircon and monazite), relative to the parent rocks (Wilford, 1995; Wilford et al., 1997; Dickson and Scott, 1997). This also allows classification of the regolith in weathering regional indexes that indicate the degree to which primary minerals have been altered to form clay minerals and oxides (Wilford, 2012; Iza et al., 2018).

Minas Gerais, Goiás, and Tocantins states in Midwest Brazil have extensive granite-greenstone terrains that host important mineral deposits (Rio das Velhas, Guarinos, Crixás, Faina and Tocantins; Cruz and Kuyumjian, 1998; Pimentel et al., 2000; Lobato et al., 2001; Jost and Fortes, 2001; Jost et al., 2010; Oliveira et al., 2004, 2015; Corrêa et al., 2015; Martins-Ferreira et al., 2017). Airborne gamma-ray spectrometry has been successfully used to identify primary Cu and Au deposits and Ni-bearing mafic-ultramafic bodies in these regions (Silva et al., 2003; Barbosa et al., 2013; Campos et al., 2017). Pires (1995) showed that Au mineralization in hydrothermal alteration zones in the Crixás deposit, Faina Greenstone Belt, were associated with anomalous concentrations of K whereas Campos et al. (2017) indicated the presence of new targets in the Faina greenstone belt.

This paper reports predictive mapping tools for mapping regoliths

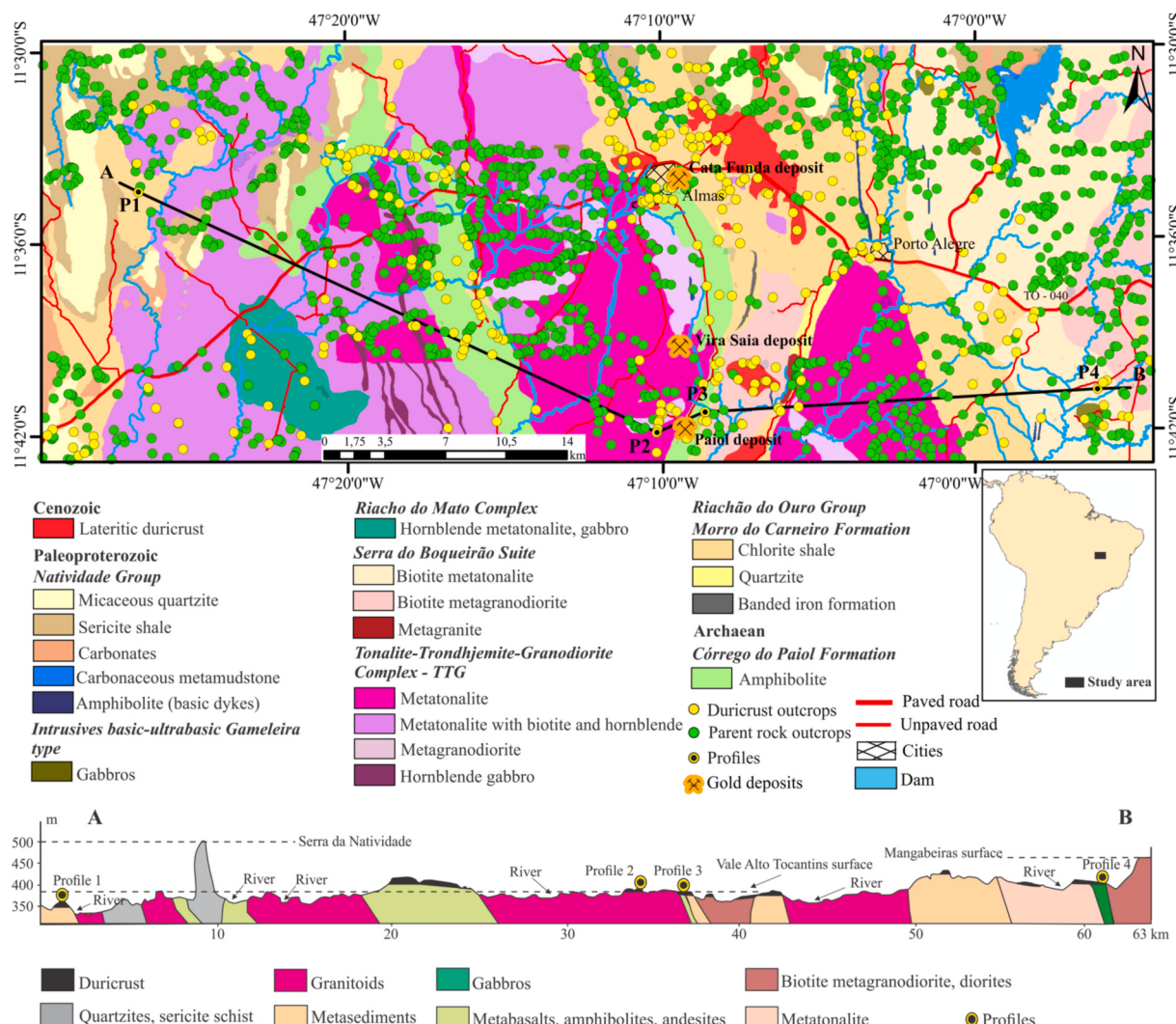


**Fig. 1.** Geological map of the study region (after CPRM, 2014 and Campos et al., 2016) and cross-section along the A–B transect. The cross-section shows the lithological units and highlights the regolith features (e.g., altitude, slope).

using airborne gamma-ray spectrometry in a granite-greenstone terrain in Midwest Brazil, which contains extensive primary Au ore deposits in saprolite and bedrock surrounded by residual lateritic duricrust (Fig. 1). As the previous maps of the Almas-Dianópolis region did not consider regolith, there was a need to reinterpret the airborne gamma-ray spectrometry data for the study area (CPRM, 2006, 2014). The study aims to develop geocomputational modeling tools that contribute to the delineation of mineral exploration targets in an area where there is a wide variety of rocks. The main contribution it provides to geosciences is that the algorithms developed to apply to differentiate areas of saprolite and parent rock from areas of lateritic duricrusts, and thus serve as a guideline for regional gold exploration. The geochemical variations of radioelements U, Th and K, measured from airborne gamma-ray spectrometry survey together with elevation data from a digital elevation model, and field outcrops observations in training sites that describe the degree of weathering, are used to generate a weathering intensity index (WII). The algorithms processed eU, eTh, K, and elevation variables in supervised classification with Boolean and fuzzy logic operators and multivariate linear regression with WII.

## 2. Geology, geomorphology, and gold mineralization

The meta-volcano sedimentary NS-trending greenstone sequence (Fig. 1) with the Sm-Nd model aged 2508 Ma, that occurs in the central part of the study region (Cruz and Kuyumjian, 1999; CPRM, 2014; Campos et al., 2016), is composed by basalt, garnet amphibolite, actinolite-chlorite schist, and andesite (Córrego do Paiol Formation) overlaid by a metasedimentary sequence of metaconglomerate, muscovite-chlorite schists, sericitic phyllite, quartzite, muscovite shale, and banded iron formation (Morro do Carneiro Formation) (Borges, 1993; Cruz and Kuyumjian, 1998; Kuyumjian et al., 2012). These two units (the Riachão do Ouro Group) are intruded by tonalite, hornblende-biotite metatonalite, biotite metagranodiorite, and hornblende gabbro plutons (TTG Complex, Serra do Boqueirão Suite, and Riacho do Mato Complex) and cut by NS-striking amphibolite and micro gabbro dikes (Fig. 1). The Rb-Sr ages of  $2050 \pm 276$  Ma and  $2217 \pm 85$  Ma provide a minimum age of granitoid intrusion in the greenstone sequence (Costa, 1985). Paleoproterozoic micaceous quartzite, sericite shale, carbonate, and carbonaceous metargillites (Natividade Group) are situated along the 500–800 m high NNE aligned hills in the central-northern and western parts of the region (Serra da Natividade, Fig. 1). The contact of all these units with the lateritic cover, which is assumed to be Cenozoic, is gradational.

Slabs, blocks, concretions, and nodules of lateritic duricrusts occur in almost the entire study region, except in the central-northern and western parts ( $>488$  m) (Oliveira and Campos, 1991; SEPLAN, 2012; CPRM, 2014; Campos et al., 2016). This sustains the undulating relief with tabular tops of the Vale do Alto Tocantins surface in the south-central part and of the Mangabeiras surface in the extreme eastern part of the study region (348–488 m high) (Figs. 1–4).

The lateritic duricrusts are reddish-brown to yellowish in color, have massive to vermicular texture, and are protopisolitic to pisolithic (profiles

1, 2, and 3 of Figs. 2–4). The lateritic duricrust consists mainly of quartz, hematite, goethite, kaolinite, gibbsite, and anatase, while having muscovite, albite, and rutile as residual minerals. However, on the gabbro, the lateritic duricrust is gray, massive, and contains todorokite, in addition to the above-mentioned minerals (manganese duricrust, profile 4 of Figs. 2 and 4C, and D). Both lateritic duricrusts are locally covered by Ferralsols and Acrisols (as per the WRB soil taxonomy WRB, 2015).

Paiol, Vira Saia, and Cata Funda are the three main gold deposits in the study region (Fig. 1). These gold deposits, classified as orogenic, shear-hosted mesothermal deposits (Cruz and Kuyumjian, 1999, 2006), are located along 15 km of the granite-greenstone terrain corridor. The Paiol deposit is well-known as gold from the saprolite was mined at an industrial scale (2 Mt of processed ore at 2.5 g/t Au) from 1996 to 2001. The gold mineralization is hosted in amphibolites with hydrothermal shear zones that are over 1400 m long, 330 m wide, and 400 m deep. The Vira Saia deposit is hosted in a metatonalitic body cut by a sinistral brittle-ductile shear zone system, and the Cata Funda deposit is hosted on saprolite, fractures, veins, and shear zones developed in metabasic and metasedimentary rocks (Martins-Ferreira et al., 2017). No gold mineralization was found in the slabs, blocks, concretions, and nodules of lateritic duricrusts.

## 3. Materials and methods

The airborne gamma-ray data used for predictive mapping were acquired from the Tocantins Aerogeophysical Project (CPRM, 2006) flown between July 2005 to January 2006, which coincides with the dry season in the region, and processed by Aerogeophysica Latinoamerica (AGP-LA) under the supervision of the Geological Survey of Brazil (CPRM). The average flight height was 100 m, with flight and control lines spaced 0.5 and 10 km apart, respectively. The aircraft was equipped with a spectrometer of 256 channels and a detector system made of sodium iodide crystals doped with thallium with 2816 cubic inches downward-looking and 512 cubic inches upward-looking detectors. The data were collected depending on flight speed on the transect, that is, approximately integrating the signal over a 75 m distance every second. In the phase prior to the airborne survey, the equipment were tested for data quality and control. Downward-looking detectors were subjected to static calibration with calibration pads and dynamic calibration with flights over dynamic calibration range (DCR) and the ocean. The conversion of counts per second (cps) to the concentration of elements was based on flights over the DCR. Upward-looking detectors were calibrated in high-level flight tests (2500 feet).

The data were corrected by AGP-LA, which adopted the recommendations of the International Atomic Energy Agency (1991). The main steps were: (a) filtering the altimeter radar data, cosmic radiation channel, and uranium to reduce the effects of high-frequency radiation; (b) correction of effective flight height based on environmental temperature and pressure; (c) removing contributions from the aircraft background and cosmic radiation components in each window of the spectrometer; (d) removal of radon background from measurements performed on the uranium window by the upward-looking detector; (e) estimation of sky shine coefficients related to uranium and thorium radiation; (f) correction of the Compton scattering; and (g) correction of altimetry based on the nominal height of the airborne survey and atmospheric attenuation.

The negative values of eU, eTh, and K concentrations, caused by the inadequate atmospheric background correction and/or instrumental calibration processes used in the Tocantins Aerogeophysical Project, were set to zero for this study. The errors in gamma-ray spectrometry data, also called dummies, although small in number and intensity can distort the results, especially when they assume negative values because the inputs used in the modeling are composed by division and multiplication of radioelements.

Airborne gamma-ray and altimetric data were further processed

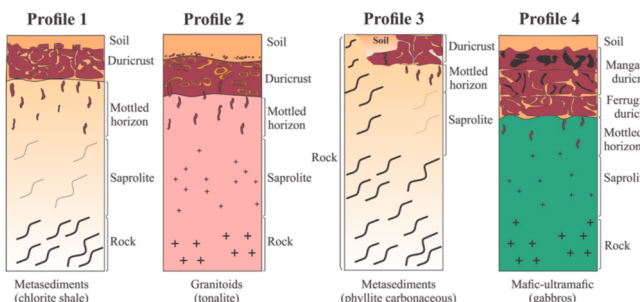
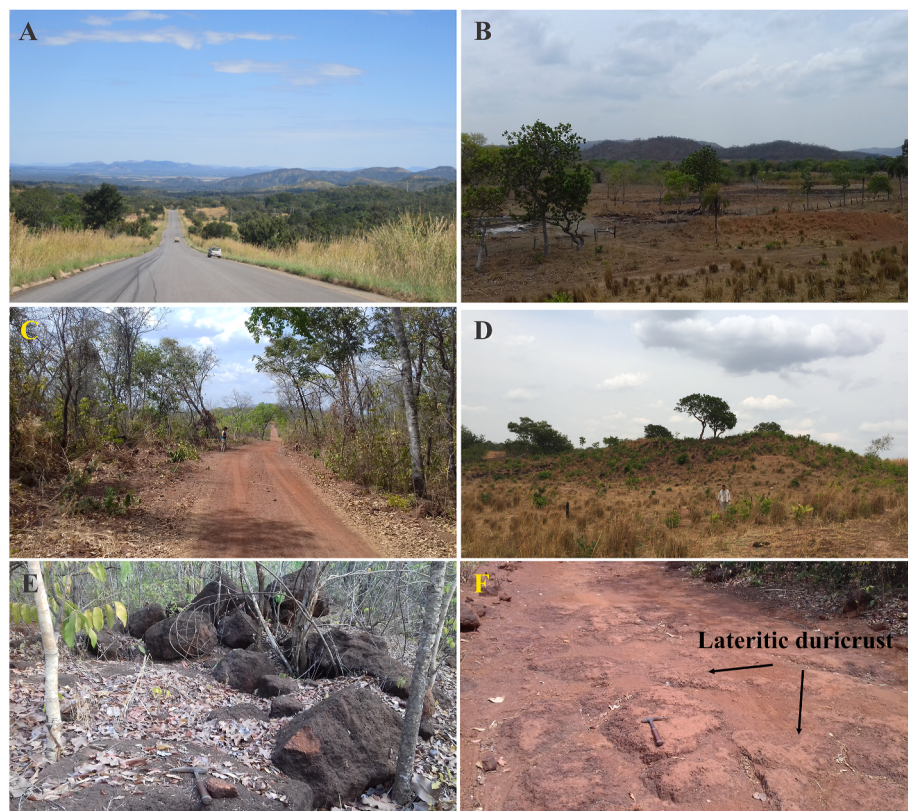


Fig. 2. Weathering lateritic profiles of the study region.



**Fig. 3.** Regolith landscape of the area. A - view of the greenstone belt (Almas-Dianópolis) highlighting hills lined up to the bottom of the landscape (Mangabeiras surface and Serra da Natividade); B - contrast between low and high relief (Mangabeiras surface) located in the southeastern part of the area; C and D - inselbergs supported by duricrust (Vale do Alto Tocantins surface); E – lateritic duricrust outcrops in blocks; and F - in slabs.

using Oasis Montaj (Geosoft) and ArcGIS (Esri) softwares. The map algebra technique based on transforming numerical data allows highlighting objects of interest on the ground surface (Carranza et al., 1999; Raines et al., 2010; Tomlin, 1994). The characteristics of these data and the way they are transformed into maps are presented in the following sections. The lateritic duricrust has the ability to retain eTh and eU in the Fe oxi-hydroxides relative to the chemical composition of the less leached substrate (saprolite and parent rock) (Wilford et al., 1997; Dickson and Scott, 1997). This allows preparation of predictive maps using airborne gamma-ray data, which when combined with other data (e.g., petrographic, geochemical, aeromagnetic, spectroscopic) can contribute as a guide for regolith studies and can indicate new target sites for ore deposits.

The airborne gamma-ray data (eU, eTh, and K channels) was re-clipped from the total region under the Tocantins Aerogeophysical Project and WGS84 was used as the spatial reference system. These data (geodatabases) were interpolated based on minimum curvature, with a 125 m grid cell size, corresponding to a quarter of the spacing between the flight lines (Fig. 5).

For the geochemical study of the regolith, 27 samples were selected from lateritic duricrust (23) and parent rock (4). They were collected in lateritic duricrust and rock slabs outcrops ( $>30 \text{ m}^2$ ) that form the tabular tops of the Vale do Alto Tocantins surface distributed throughout the study region. No samples were collected in the incised valley and riverbed because lateritic duricrusts were not found in these locations. The samples were dried in an oven ( $60^\circ\text{C}$ ), pulverised, and extracted as aliquots for chemical and mineralogical analysis. Chemical analyses were performed by ALS-Laboratory Services. The major elements ( $\text{SiO}_2$ ,  $\text{Al}_2\text{O}_3$ ,  $\text{Fe}_2\text{O}_3$ ,  $\text{TiO}_2$ ,  $\text{MgO}$ ,  $\text{CaO}$ ,  $\text{Na}_2\text{O}$  e  $\text{K}_2\text{O}$ ,  $\text{P}_2\text{O}_5$ , and  $\text{MnO}$ ) were analyzed by ICP-ES after fusion with  $\text{LiBO}_2$  and loss to fire (LOI) by gravimetry. The Th and U were analyzed by ICP-MS. The minerals were identified by X-ray diffraction (RIGAKU IV equipped with a Cu tube) in

the laboratory of Universidade de Brasília (UnB).

### 3.1. Boolean and fuzzy logics applied to regolith mapping

Techniques based on Boolean and fuzzy logic operations are used in the construction of knowledge-driven models, i.e., models based on previous information or hypotheses made by an expert (Bonham-Carter, 1994). Boolean logic consists of applying mathematics to human reasoning. It uses the classical theory of sets, in which an element is or is not a part of a set. Logical complementation (NOT), logical multiplication (AND), and logical addition (OR) are the operations that are applied to a data set. The Index Overlay Method (IOM), associated with this logic, allows assigning different weights to the variables while the average normalized by the sum of weights (weight-weighted average) allows identifying the influence of each variable in binary (0 or 1) format (Bonham-Carter, 1994). The resulting maps allow to differentiate exposed areas of parent rock and saprolite from areas with lateritic duricrusts. It is emphasized that the prior traditional mapping of the region was essential for guiding the study. The choice of data, the kinds of information extracted from it, and the assignment of weights to evidence were dependent on the environment regional (Midwest Brazil context). For example, vegetation map was not employed, because it is not directly useable as lateritic duricrust evidence; as well as lower weight assigned to elevation relative to the airborne gamma-ray data, because lateritic duricrust had been observed over a relatively wide range of altitudes.

Fuzzy or diffuse logic is an outgrowth theory of sets (Zadeh, 1965), where the transition between favorable and non-favorable areas can be gradual rather than abrupt (Boolean logic), assuming any value in the interval between 0 and 1. The membership function of a fuzzy set A is denoted by  $\mu_A(x)$  and usually has the form  $\mu_A: X \rightarrow [0, 1]$ , where X is the universal set under consideration and A is a label of the fuzzy set defined



**Fig. 4.** Lateritic duricrust textures. A - vermicular to protonodular; B - vermicular; C - manganese vermicular; D - vermicular and massive manganese; E – pisolithic; and F - vermicular with botryoidal goethite.

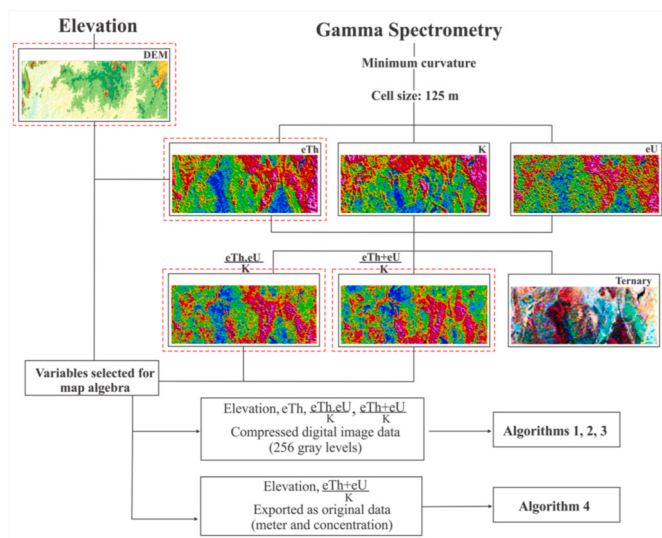


**Fig. 5.** Data processing flowchart and alternative products from algorithms 1, 2, 3 and 4. Respective colorbars of K, eTh, and eU are presented in Fig. 7.

by this function. The universal set is always assumed to be a crisp set A. For each  $x \in X$ , the value  $\mu_A(x)$  expresses the degree of membership of element x of X in the fuzzy set A. Each fuzzy membership function (e.g., large, small, Gaussian, linear) varies with the equation and application while the choice is based on the option that best captures the

transformation of the data based on the phenomenon being modeled. The fuzzy large function is used when input values are greater than the defined midpoint (assigned to an association of 0.5), which indicates a greater possibility of being members of the set and values below the midpoint with a decreasing membership (Fig. 6A). The fuzzy small function is the opposite. It is used when the smaller input values are more likely to be a member of the set. Values greater than the midpoint indicate a lower possibility of being a member of the set and values below the midpoint indicate a higher possibility of the membership (Fig. 6B). Fuzzification is the process of converting a crisp input value to a fuzzy value, and is conducted using the information in the knowledge base, while defuzzification is the return to the classic mathematical set (Zadeh, 1965; Zimmermann, 1985). The crisp input value can assume in classification the raw data (e.g., radioelement concentrations) or compressed digital image data (e.g., 8-bit), among other possibilities. These two input data approaches were analyzed in this study to compose the classification algorithms.

Boolean logic uses the Boolean operator '&' (AND), algebraic operator '+', and different weight combinations, for example, 1 for elevation and 4 for  $\frac{eTh+eU}{K}$  (IOM). Thus, the different weights are arranged in a geometric progression of common ratio 4;  $(A_n = 4^{n-1}):(1 * \text{elevation} + 4 * \frac{eTh+eU}{K})/5$  (Iza et al., 2016). These were the criteria applied to define weighting parameters of the variables, which allowed the best discrimination of lateritic duricrusts, mottled horizon, and soil areas. Fuzzy logic uses the fuzzy operators: Fuzzy Algebraic Product Operator (FAPO) to minimize the results, Fuzzy Algebraic Sum Operator (FASO) to maximize the results, and Fuzzy Gamma Operator (FGO) to balance the results. The FAPO tends to be very small with this operator due to

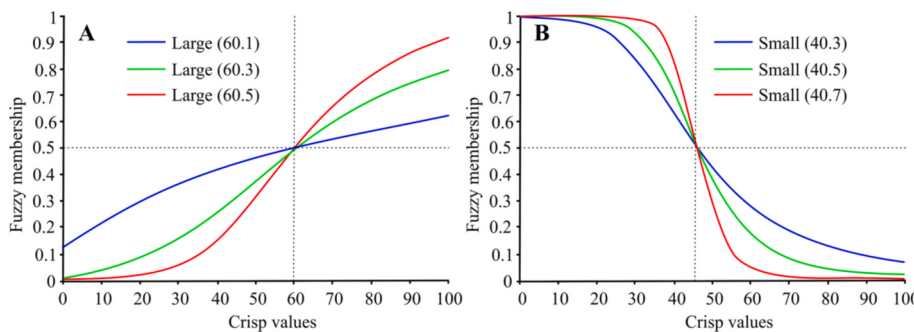


**Fig. 6.** Fuzzy membership functions. A - Fuzzy large function and B - Fuzzy small function.

multiplication of several numbers less than 1. The output is always smaller than, or equal to, the smallest contributing membership value, and is therefore “decreasive”. In the FASO, the result is always larger than (or equal to) the largest contributing fuzzy membership value, and the effect is therefore “increasive”. Two pieces of evidence, both favoring a hypothesis, reinforce each other and the combined evidence is more supportive than either piece of evidence taken individually. FGO is the combination of FAPO and FASO. Details regarding these operators can be found in Zadeh (1965), Zimmermann (1985), Bonham-Carter (1994), Klir (2004), Eddy et al. (2006), and Nykänen et al. (2008). Each operator generated a predictive map in the raster calculator and the results were compared to those from the fuzzy large pertinence function (fuzzification) in the GIS software. The fuzzy large function was used as the larger input values are more likely to be a member of the fuzzy set. In this study, the data were divided into five classes: extremely unfavorable, unfavorable, moderately favorable, favorable, and extremely favorable (Wilford, 2012; Iza et al., 2016). The first two classes were assigned to parent rock and saprolite, while the last two were assigned to lateritic duricrust and its dismantling products, and the moderately favorable class was assigned to the mottled horizon where lateritic duricrust fragments are not uncommon. The number of classes most appropriate for the study region was defined by observing the weathering stages of the field outcrops.

### 3.2. Algorithms validation

The efficiency of the predictive mapping results expressed by the kappa coefficient ( $\kappa$ ), is defined as  $\kappa = (p_0 - p_e)/(1 - p_e)$ , where  $p_0$  indicates the observed agreement,  $p_e = [(n_1/n) * (m_1/n)] + [(n_0/n) * (m_0/n)]$  is the expected agreement,  $m_1$  is total parent rock outcrops,  $m_0$  is total duricrust outcrops,  $n_1$  is total parent rock prediction,  $n_0$  is total duricrust prediction, and  $n$  is total field outcrops. Table 1 schematically illustrates how kappa coefficient are calculated. Part of the observed agreement is attributed to chance, making it larger than the expected agreement ( $p_0 > p_e$ ). Kappa is a measure of this difference, standardized to lie on a  $-1$  to  $1$  scale.  $\kappa$  is intended to provide a quantitative measure of the magnitude of the agreement among the lithological information

**Table 1**

Confusion matrix used to measure the agreement between field outcrops observations and predictive map (adapted from Cohen, 1960 and Viera and Garrett, 2005).

		Predictive map		
		Parent rock	Duricrust	Total
Field outcrops observations	Parent rock	A	B	$m_1$
	Duricrust	C	D	$m_0$
	Total	$n_1$	$n_0$	$n$

Note<sup>1</sup>. a = parent rock predicted as parent rock; b = parent rock predicted as duricrust; c = duricrust predicted as parent rock; d = duricrust predicted as duricrust;  $n_1 = a + c$ ;  $n_0 = b + d$ ;  $m_1 = a + b$ ;  $m_0 = c + d$ ; n = total field outcrops.

predicted by the model and its nature (e.g., parent rock or lateritic duricrust) confirmed in field outcrop (Cohen, 1960; Viera and Garrett, 2005). Kappa values between 1 and 0.81 indicate almost perfect agreement, between 0.80 and 0.61 indicate substantial, between 0.60 and 0.41 indicate moderate, and values closer to 0 indicate lower agreement (Landis and Koch, 1977). For this study, 1745 field outcrops were recorded, of which 1462 were assigned as parent rock (rock and saprolite) and 283 as lateritic duricrust (mottled horizon, soil and duricrust) in four possibilities: a) concordant lateritic duricrust; b) discordant lateritic duricrust; c) discordant parent rock; and d) concordant parent rock, which are the basis for determining  $\kappa$ . The supervised classification method was adopted in this study.

### 3.3. Multivariate linear regression

The gamma-ray spectrometric signature via multivariate linear regression is another way for mapping the regolith (Wilford, 2012; Iza et al., 2018) quicker than logic tools. To use this technique, the 1745 mapped sites were grouped in weathering classes (WCs) according to field observations in the study region: 1) unweathered, 2) slightly weathered, 3) moderately weathered, 4) highly weathered, and 5) extremely weathered (Table 2), where the last three classes included lateritic duricrust (mottled horizon, soil and duricrust). Statistical parameters (average, maximum, minimum, and standard deviation) and Pearson correlation coefficient ( $r$ ) were calculated for elevation, eTh, eU, K,  $\frac{eTh \cdot eU}{K}$ , and  $\frac{eTh + eU}{K}$  for each of the five WCs (Table 2). The Pearson correlation coefficient intervals were classified as weak ( $0$  to  $\pm 0.29$ ), moderate ( $\pm 0.30$  to  $\pm 0.49$ ), and strong ( $\pm 0.50$  to  $\pm 1.00$ ) according to Cohen (1988), and the multivariate regression was conducted according to the backward model stepwise regression of Wilford (2012). This approach identifies the independent variables that most influence the variability in the WC, the dependent variable. In the final step, the independent variables, eTh, eU,  $\frac{eTh \cdot eU}{K}$ ,  $\frac{eTh + eU}{K}$ , and elevation were used in the weathering intensity index (WII) equation and the map was compared to the Boolean and FAPO predictive maps.

## 4. Results

### 4.1. Exploratory data analysis

The total count image of gamma rays emitted by K, Th, and U reflected on the RGB space (Fig. 7A, B, and C), which when combined, resulted in the ternary map shown in Fig. 7D. The lateritic duricrusts occur along the greenish areas identified by high eTh and eU concentrations and low K content (Fig. 7D), especially in the manganese lateritic duricrust, relative to other rocks (Table 3). The central-northern, northwestern, and northeastern parts (whitish colors, Fig. 7D) have zones with high eTh (red to pink color, Fig. 7B) encompassed by high K (red to pink color, Fig. 7A). These zones mark the domain of metatonalites and metagranodiorites (Serra do Boqueirão Suite and TTG), saprolite and the rare lateritic duricrust outcrops

**Table 2**

Classification of the weathering level of the regolith adapted for the study region (Wilford, 2012; Iza et al., 2018).

Level (WC)	Weathering intensity	Descriptions
1	Unweathered	Rock without signs of decomposition, structure and preserved primary mineralogy. Rock outcrops predominate over soils (>70%). Surface soils when present are Gleysols.
2	Slightly weathered	Rock slightly discolored with eventual staining. The overall fabric of the rock is well preserved, and outcrop are common. Primary minerals are largely preserved; however, feldspars can be slightly weathered. Surface soils are typically Cambisolos.
3	Moderately weathered	Residual sands and clays are common in the upper part of the weathering profile. Rock partially weathered but still cohesive. Most of the feldspars are weathered. Profile commonly mottled. Lateritic duricrusts are not uncommon. Surface soils are typically Plinthosols. Absence of a layer of accumulated clay, humus or soluble salts.
4	Highly weathered	Residual sands and clays are common in the upper part of the weathering profile. Profile commonly mottled with the primary bedrock structure typically lost. Saprolite soft and weakly cohesive that can be broken by hand. The mineral content is dominated by clays, oxi-hydroxides of iron and aluminum with or without residual quartz and anatase. Other minerals in low abundance or absent. Blocks and slabs of lateritic duricrusts, lateritic gravels, Acrisols and Ferralsols dominate rock outcrops (>80%).
5	Extremely weathered	Residual sands and clays are common in the upper part of the weathering profile; mottling and leaching are intense and frequent. Saprolite is soft with primary minerals completely weathered to form clays or oxi-hydroxides. However, resistant quartz veins may still remain together with the anatase as the only remaining primary minerals. Blocks and slabs of lateritic duricrust, lateritic gravels, Acrisols and Ferralsols are dominates (>95%). Practically no parent rock appears.

(Fig. 1). The darker areas (Fig. 7D) are characterized by low eTh and eU (cyan, Fig. 7B and C), whereas the reddish colors correspond to parts of the TTG domain (Fig. 1). In some of these sites in the midwestern region, the existing lateritic duricrusts (Fig. 7D) did not show a tendency to concentrate Th and U.

The preliminary analysis illustrated the gamma-ray spectrometry signature of the study region. Thereafter, several combinations of data variables were used in the predictive mapping experiments, along with data transformations (with or without previous data reclassification, raw, and 8-bit image) and modeling methods (Boolean, Fuzzy, and multivariate regression). The individual Th channel, and the  $\frac{eTh}{K}$  and  $\frac{eTh+eU}{K}$  ratios were used to highlight the signature of the lateritic duricrust (high eTh and eU relative to K values) (Wilford et al., 1997; Carrino et al., 2011; Iza et al., 2016). The Pearson correlation coefficient of  $\frac{eTh+eU}{K}$  relative eTh and eU in the lateritic duricrusts (0.74 and 0.58, respectively) was slight higher than the coefficients in the bedrock and saprolite (0.60 and 0.53, respectively), highlighting the suitability of  $\frac{eTh+eU}{K}$  ratio for mapping regoliths (Fig. 8). The average  $\frac{eTh+eU}{K}$  in the lateritic duricrusts (9.05) was higher than that in the parent rock and saprolite (6.07). The Pearson correlation coefficient of  $\frac{eTh+eU}{K}$  relative to eTh and eU in the lateritic duricrusts (0.83 and 0.76, respectively) was similar to the coefficients for bedrock and saprolite (0.81 and 0.75, respectively). The average  $\frac{eTh+eU}{K}$  in the lateritic duricrust (19.6) was also higher than that in the parent rock and saprolite (11.17) (Fig. 8).

#### 4.2. Boolean and fuzzy logic

Several combinations of airborne gamma-ray were tested. Fig. 5 shows the flowchart with the four algorithms applied to data to obtain the regolith predictive maps for the study area (Table 4): algorithm 1 - eTh exported from GIS software as an 8-bit image (256 Gy levels) processed with elevation (8-bit) using the Boolean (AND) and fuzzy operators (FAPO, FASO, and FGO); algorithm 2 -  $\frac{eTh+eU}{K}$  processed with elevation and exported according to algorithm 1; algorithm 3 -  $\frac{eTh+eU}{K}$  exported in the same format as that of algorithm 1 and elevation, applying the Boolean IOM and different weights (1 for elevation and 4 for  $\frac{eTh+eU}{K}$ ) (Bonham-Carter, 1994), and applying the fuzzy method (Zadeh, 1965) to these variables; and algorithm 4 - the same variables as of algorithm 3, but used the raw data (not compressed digital image) including elevation, and exported from GIS software with the appropriate extension (.flt) to maintain the original data in concentration, and then applying the Boolean IOM and fuzzy (see Figs. 9 and 10, respectively) methods.

In each algorithm, the topographic altitudes of the lateritic duricrust (348–488 m), defined by the SRTM images and fieldwork, were used in the raster calculator to generate a Boolean predictive map of elevation by applying the AND operator in the expression [elevation  $\geq (\bar{X} - \sigma)$ ] AND [elevation  $\leq (\bar{X} + 3/2 \sigma)$ ] for both raw elevation data and compressed digital image data, where  $\bar{X}$  is the average and  $\sigma$  the standard deviation (Table 5). The Boolean predictive maps of airborne gamma-ray data were prepared using the expressions: [eTh  $\geq (\bar{X} + 1/3 \sigma)$ ] (algorithm 1); [ $\frac{eTh+eU}{K} \geq (\bar{X} + 1/3 \sigma)$ ] (algorithm 2); [ $\frac{eTh+eU}{K} \geq (\bar{X} + 1/3 \sigma)$ ] (algorithm 3); and [ $\frac{eTh+eU}{K} \geq \bar{X}$ ] (algorithm 4, Table 5).

The combinations of airborne gamma-ray and altimetric data using algebraic operators ( $-$ ,  $+$ ,  $\geq$ , and  $\leq$ ) and Boolean logic (AND) resulted in Boolean predictive maps that highlighted the areas favorable and non-favorable for lateritic duricrusts (Fig. 9). The elevation increased the accuracy (91%) and  $\kappa$  (0.69) of the Boolean prediction (algorithm 4) relative to  $\frac{eTh+eU}{K}$  (accuracy 87%;  $\kappa = 0.56$ ). The fuzzification of the FAPO, FASO, and FGO formulas (Table 4) yielded fuzzified maps (Fig. 10). The five classes in the fuzzy predictive maps (extremely unfavorable, unfavorable, moderately favorable, favorable, and extremely favorable) were based on their histograms and field outcrops observations. The classes with lower values (extremely unfavorable and unfavorable) corresponded to areas of parent rock and saprolite, whereas classes with the three highest values (moderately favorable, favorable and extremely favorable) corresponded to areas of mottled horizon, soil and lateritic duricrust (Wilford, 2012; Iza et al., 2016). The maps that best predicted (Fig. 11) the lateritic duricrusts relative to the parent rocks and saprolites, were the Boolean and FAPO prepared under algorithm 4 (Fig. 11A and B, respectively) using  $\frac{eTh+eU}{K}$  and the raw data (Figs. 9 and 10, respectively). Similar to elevation, eU cannot be disregarded in the predictive mapping for the study region. It combined in  $\frac{eTh+eU}{K}$  improves the results (accuracy 90%;  $\kappa_{FAPO} = 0.66$ ) in relation to eTh/K single ratio (accuracy 86%;  $\kappa_{FAPO} = 0.50$ ).

#### 4.3. Weathering intensity index

The Pearson correlation coefficient showed that the correlations between the elevation, eTh, eU, K, and  $\frac{eTh+eU}{K}$  (Table 6) and the five WCs were strong for eTh ( $r = 0.58$ , Table 7), eU ( $r = 0.52$ ), and  $\frac{eTh+eU}{K}$  ( $r = 0.76$ ), and weak for elevation ( $r = 0.18$ ) and K ( $r = -0.12$ ), as per the classification by Cohen (1988) (Table 7). Although the correlation coefficient between elevation and WC was weak, the kappa coefficient (0.58) and field outcrops observations indicated that elevation is an important factor for regolith mapping in the study region (Table 4).

The parameters Th,  $\frac{eTh+eU}{K}$ , and elevation explained 62.4% of WC variability with the correlation intensity of  $r = 0.79$  (Table 8). These

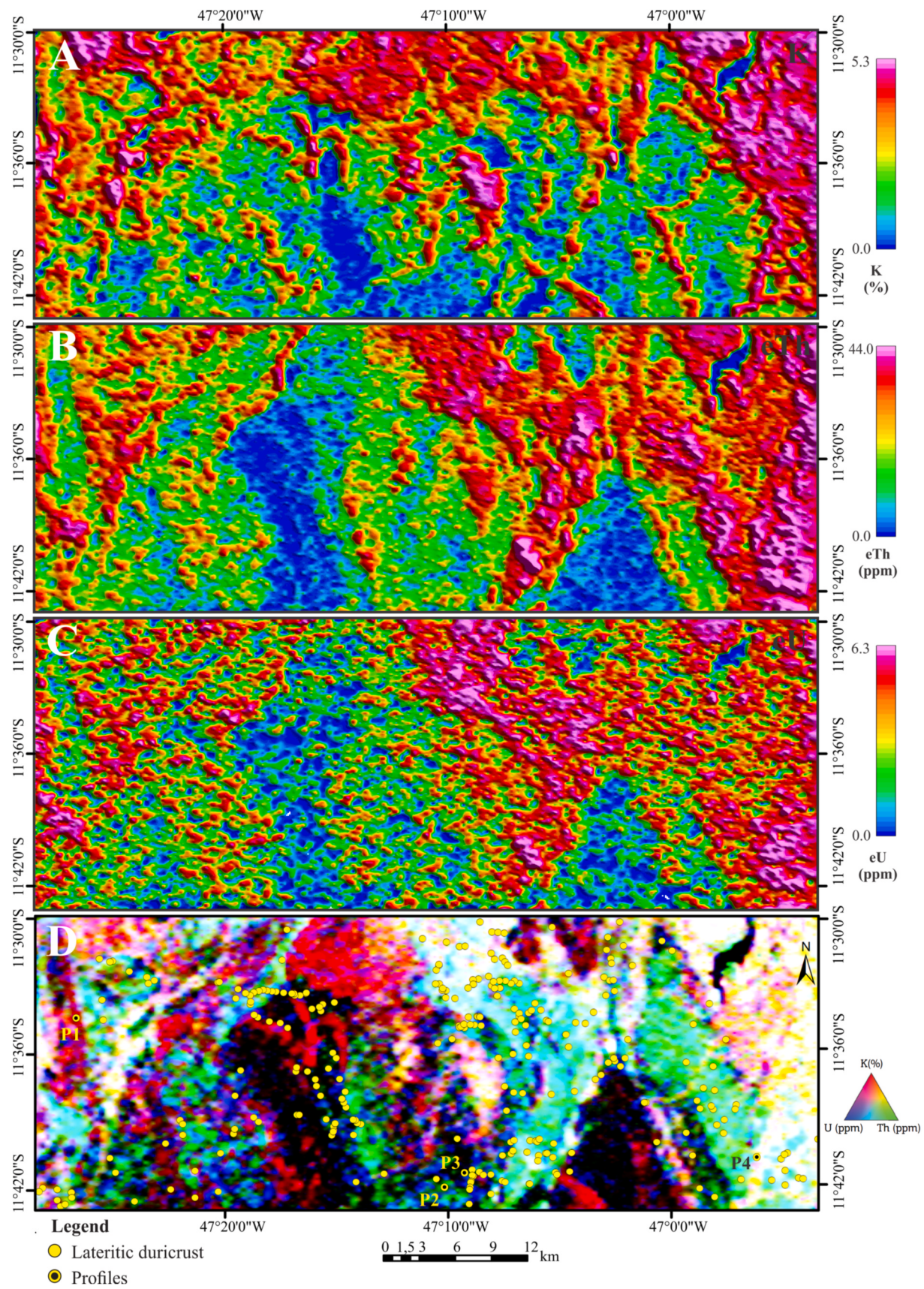


Fig. 7. Airborne radio-element grids of the individual channels and RGB ternary composition of gamma-ray spectrometric data (K, eTh, and eU).

**Table 3**

Average chemical composition of the lateritic duricrust and rocks, K in % and Th and U in ppm. Estimates of uranium and thorium concentrations are reported as uranium equivalent (eU) and thorium equivalent (eTh).

Average	Chemical composition			Gamma-ray spectrometry		
	K	Th	U	K	eTh	eU
Ferruginous lateritic duricrust	0.2	6.8	2.1	1.3	8.9	2.4
Manganese lateritic duricrust	0.2	12.7	4.1	1.8	28.8	4.6
Parent rock	0.7	2.6	0.5	1.7	8.0	2.2

variables when integrated by multivariate linear regression resulted in a global p-value of 0.00 for the F test ( $<0.05$ ). This implies that at least one of the variables was correlated with WCs (Table 8). Despite the strong correlation of WC with eU ( $r = 0.52$ ), eU had a p-value of 0.36 for the F test ( $>0.05$ ) in multivariate linear regression. This indicated multicollinearity between eU and other variables (Th,  $\frac{eTh+eU}{K}$ , and elevation) and eU was not used for calculating WII. All three statistically significant (individual p-values  $< 0.05$ ) variables (Th,  $\frac{eTh+eU}{K}$ , and elevation) in the multivariate linear regression were used to generate the WII equation (Equation (1)) and the predictive regolith map for the study region (Fig. 12).

$$WII = -1.2810 + 0.0034 \cdot \text{elevation} + 0.0310 \cdot eTh + 0.2327 \cdot \frac{eTh+eU}{K} \quad (1)$$

The duricrust lateritic areas are underestimated when they are used in the WII map and in the FAPO map's four classes (unfavorable, moderately favorable, favorable, and extremely favorable) instead of five classes (extremely unfavorable, unfavorable, moderately favorable, favorable, and extremely favorable). The kappa coefficient decreased from 0.66 to 0.52 as many parent rock outcrops were classified in FAPO as lateritic duricrust.

## 5. Discussion

Algorithms with different combinations of variables were tested. The degree of rocks alteration in 1745 field outcrops; the parent rocks and

lateritic radioelements signatures proposed in the literature, in addition to other possibilities; and the kappa coefficient were the criteria adopted to determine the efficiency of the predictive mapping results. The algorithm 4:  $(\frac{eTh+eU}{K})$  exported with appropriate extension to maintain the original data in concentration and elevation with  $\kappa_{\text{Boolean}} = 0.69$  and  $\kappa_{\text{FAPO}} = 0.66$  was found to have the most accurate mathematical approach (substantial efficiency; accuracy 91%) for regolith mapping (Table 4 and Fig. 11). This indicates that despite the great variety of rocks covered by sparse shrubs, it was possible to identify the spreading lateritic duricrusts (mottled horizon, soil and duricrust) that covers almost 30% of the total area (Table 4 and Fig. 11). This area is larger than the areas delimited by previous geological mappings (CPRM, 2014; Campos et al., 2016, Fig. 1). Although the low eU concentration ( $\bar{X} = 2.2$  ppm, Table 6) when it is combined in  $\frac{eTh+eU}{K}$  algorithm (4) it improves the accuracy to 90% and the  $\kappa_{\text{FAPO}}$  to 0.66 relative to  $eTh/K$  (accuracy 86%;  $\kappa_{\text{FAPO}} = 0.50$ ). The altitude range (348–488 m) is an important variable for the lateritic duricrusts identification, as indicated Iza et al. (2018). In the study area it improves the accuracy (91%) and  $\kappa_{\text{Boolean}}$  (0.69) of predictive maps to relative to those generated by algorithms using only  $\frac{eTh+eU}{K}$  (accuracy 87%;  $\kappa_{\text{Boolean}} = 0.56$ ), and therefore their quality.

The weak to moderate efficiency ( $\kappa \leq 0.48$ ) and low accuracy ( $\leq 79\%$ ) of algorithms 1, 2, and 3 to identify the lateritic duricrusts (Table 4) resulted in a three-fold increase in the number of discordant parent rocks (parent rock and saprolite) of the model (parent rock predicted as duricrust). Further, algorithm 2 ( $\kappa_{\text{FGO}} = 0.10$ ), that used the  $\frac{eTh+eU}{K}$  ratio, was less efficient than algorithm 3 ( $\kappa_{\text{FGO}} = 0.34$ ) that used the  $\frac{eTh+eU}{K}$  ratio. The integration of raw data of  $\frac{eTh+eU}{K}$  and elevation was also tested. Although the average  $\frac{eTh+eU}{K}$  (19.6) in lateritic duricrusts was greater than average  $\frac{eTh+eU}{K}$  (9.05), the predictive maps had moderate efficiency ( $\kappa_{\text{Boolean}} = 0.55$  and  $\kappa_{\text{FAPO}} = 0.43$ ) due to excessive restriction of the lateritic duricrust areas. The  $\frac{eTh+eU}{K}$  ratio most accurately predicted areas with lateritic duricrusts.

The mathematical logic (Fig. 11) and multivariate linear regression (Fig. 12) showed the efficiency of the airborne gamma-ray spectrometry in mapping regoliths in the Midwest Brazil. The Boolean (91%) and FAPO (90%) are excellent predictive techniques and were marginally more accurate than multivariate regression WII techniques (88%) for the

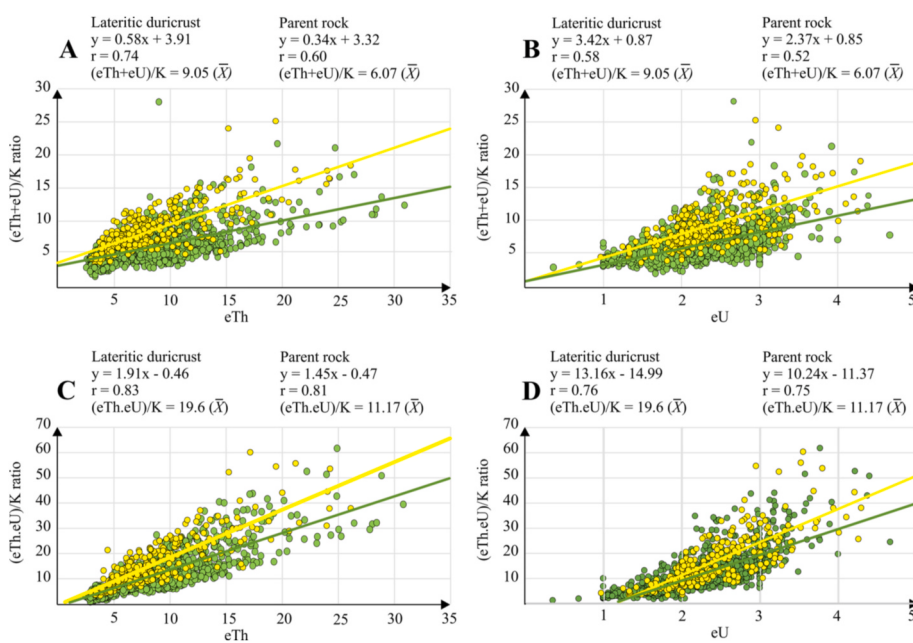


**Fig. 8.** Plots of gamma-ray spectrometric signatures of lateritic duricrust (yellow dots) relative to those of parent rock (green dots): A –  $(eTh + eU)/K$  vs. eTh; B –  $(eTh + eU)/K$  vs. eU; C -  $(eTh.eU)/K$  vs. eTh; and D -  $(eTh.eU)/K$  vs. eU. K (%), Th (ppm), U (ppm).

**Table 4**

Results of the predictive maps for favorable and extremely favorable areas to the occurrence of lateritic duricrusts using different variables and processing flows. The algorithm used in Boolean and fuzzy predictions maps (4) have the best accuracy and kappa coefficient ( $\kappa$ ).

Input	Logic	Formulas and data type	Confusion matrix*	Accuracy (%)	$\kappa$	Area (%)**
Compressed digital image data (0–255)						
1 eTh	Elevation (SRTM)	Boolean	Elevation AND eTh	(935-527-66-217)	66	0.25
		FAPO	Elevation* $eTh$	(768-694-51-232)	57	0.18
		FASO	(1-(1-Elevation)*(1- $eTh$ ))	(814-648-52-231)	60	0.20
		FGO	Power ((FASO),0.7)*Power ((FAPO),0.3)	(501-961-10-273)	44	0.13
Compressed digital image data (0–255)						
2 $\frac{eTh \cdot eU}{K}$	Elevation (SRTM)	Boolean	Elevation AND $\frac{eTh \cdot eU}{K}$	(1083-379-29-254)	77	0.43
		FAPO	Elevation* $\frac{eTh \cdot eU}{K}$	(1003-459-19-264)	73	0.38
		FASO	(1-(1-Elevation)*(1- $\frac{eTh \cdot eU}{K}$ ))	(971-491-20-263)	71	0.36
		FGO	Power ((FASO),0.7)*Power ((FAPO),0.3)	(403-1059-4-279)	39	0.10
Compressed digital image data (0–255)						
3 $\frac{eTh + eU}{K}$	Elevation (SRTM)	Boolean (IOM)	$(1 * Elevation) + (4 * \frac{eTh + eU}{K}) / 5$	(1124-338-20-263)	79	0.48
		FAPO	Elevation* $\frac{eTh + eU}{K}$	(959-503-12-271)	70	0.36
		FASO	(1-(1-Elevation)*(1- $\frac{eTh + eU}{K}$ ))	(962-500-39-244)	69	0.31
		FGO	Power ((FASO),0.7)*Power ((FAPO),0.3)	(986-476-34-249)	71	0.34
Raw data (in concentration and meter)						
4 $\frac{eTh + eU}{K}$	Elevation (SRTM)	Boolean (IOM)	$(1 * Elevation) + (4 * \frac{eTh + eU}{K}) / 5$	(1352-110-51-232)	91	0.69
		FAPO	Elevation* $\frac{eTh + eU}{K}$	(1366-96-73-210)	90	0.66
		FASO	(1-(1-Elevation)*(1- $\frac{eTh + eU}{K}$ ))	(1364-98-73-210)	90	0.65
		FGO	Power ((FASO),0.7)*Power ((FAPO),0.3)	(1362-100-74-209)	90	0.65

Note<sup>2</sup>. \* Respective values for parent rock predicted as parent rock, parent rock predicted as duricrust, duricrust predicted as parent rock and duricrust predicted as duricrust.

\*\*Area covered by lateritic materials (lateritic duricrust, mottled horizon and soil).

FAPO - Fuzzy Algebraic Product Operator, FASO - Fuzzy Algebraic Sum Operator, FGO - Operator Gamma Fuzzy.

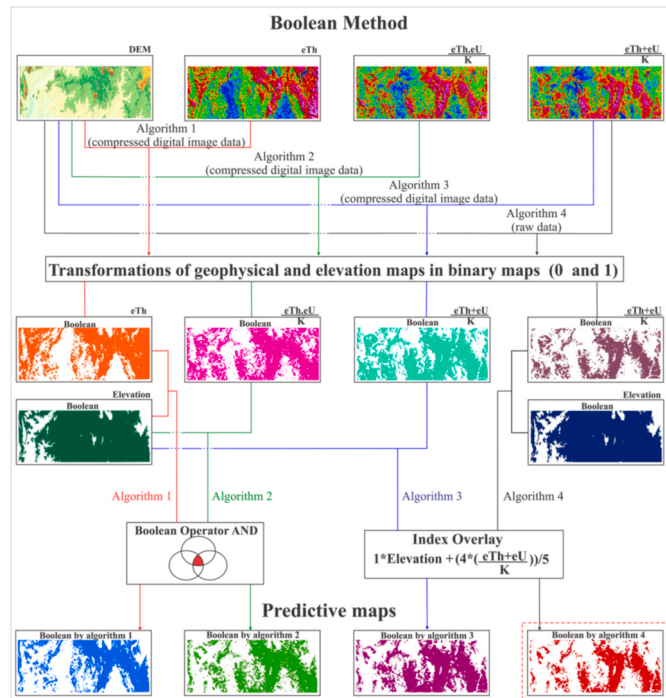


Fig. 9. Flowchart of the algorithms for generating Boolean predictive maps.

study region (Figs. 11 and 12). However, calculating WII is faster as it requires less mathematical processing and is simpler to work with as it

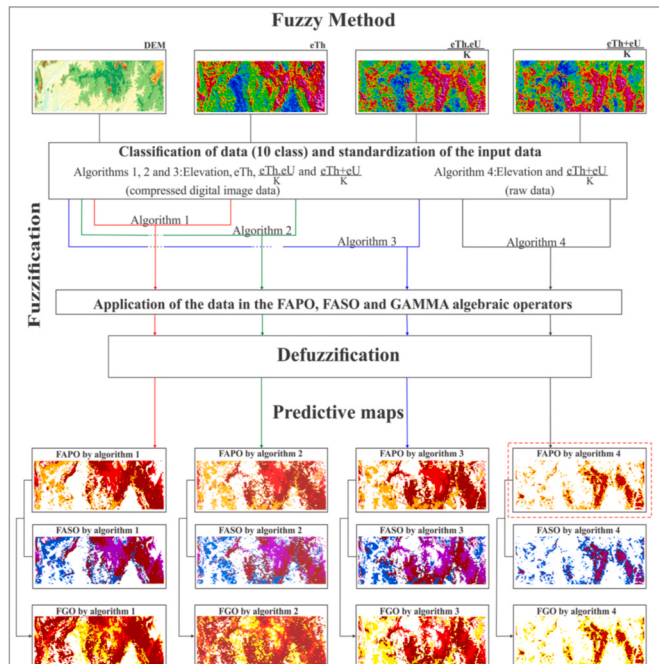


Fig. 10. Flowchart of the algorithms for generating fuzzy predictive maps.

uses basic statistical methods. Thus, the techniques used to prepare regolith maps suitable to discriminate areas of parent rock and saprolite from areas with lateritic duricrusts can help as a guide in the prospecting

**Table 5**

Statistical summary of  $e\text{Th.eU}/K$ ,  $e\text{Th} + e\text{U}/K$  and elevation for the algorithms 1, 2, 3, 4.

Algorithms	Variables	Min	Max	Average ( $\bar{X}$ )	Standard deviation ( $\sigma$ )
1 *	$e\text{Th}$	0.0	255.0	152.9	97.8
2 *	$e\text{Th.eU}/K$	0.0	255.0	154.9	97.4
3 *	$e\text{Th} + e\text{U}/K$	0.0	255.0	154.7	97.5
(1, 2, 3) *	Elevation	0.0	255.0	46.9	26.7
4 ***	$e\text{Th} + e\text{U}/K$	1.0	111.6	7.0	3.5
4 ***	Elevation	314.0	772.0	404.0	51.5

Note<sup>3</sup>. \* Compressed digital image data (0–255). \*\* Raw data:  $e\text{Th}$  (ppm),  $e\text{U}$  (ppm), K (%), elevation (m).

of new targets for mineral exploration in the region.

The combined use of a wide range of data layers (e.g., lateritic index - LI, WII, digital elevation model - DEM, and geochemical map) is now a standard method of automated routines for visualizing the spatial distribution of regolith and landforms in Australia and other countries

(Carranza et al., 1999; Wilford, 2012; Metelka et al., 2018). More informative maps can be created as layers in the GIS software and can help with the planning of further geochemical investigations and construction of complex thematic maps (Craig, 2001). There are several combinations of airborne gamma-ray data:  $e\text{Th}/K$ ,  $e\text{U}/K$  (Iza et al., 2016), and LI ( $\frac{e\text{Th.eU}}{K^2}$ ) (Iza et al., 2018). However, they underestimate or overestimate the predicted areas for lateritic duricrusts. The size of the lateritic duricrust outcrops also affects the efficiency of airborne

**Table 6**

Basic statistics of altimetric and airborne gamma-ray data at observed sites (algorithm 4, raw data).

	N	Minimum	Maximum	Average ( $\bar{X}$ )	Standard deviation ( $\sigma$ )
Elevation (m)	1745	320	637	410.2	46.6
$e\text{Th}$ (ppm)	1745	2.5	30.9	8.2	4.0
$e\text{U}$ (ppm)	1745	0.4	4.7	2.2	0.5
K (%)	1745	1.0	4.0	1.7	0.6
$e\text{Th} + e\text{U}/K$	1745	1.6	28.0	6.6	2.8

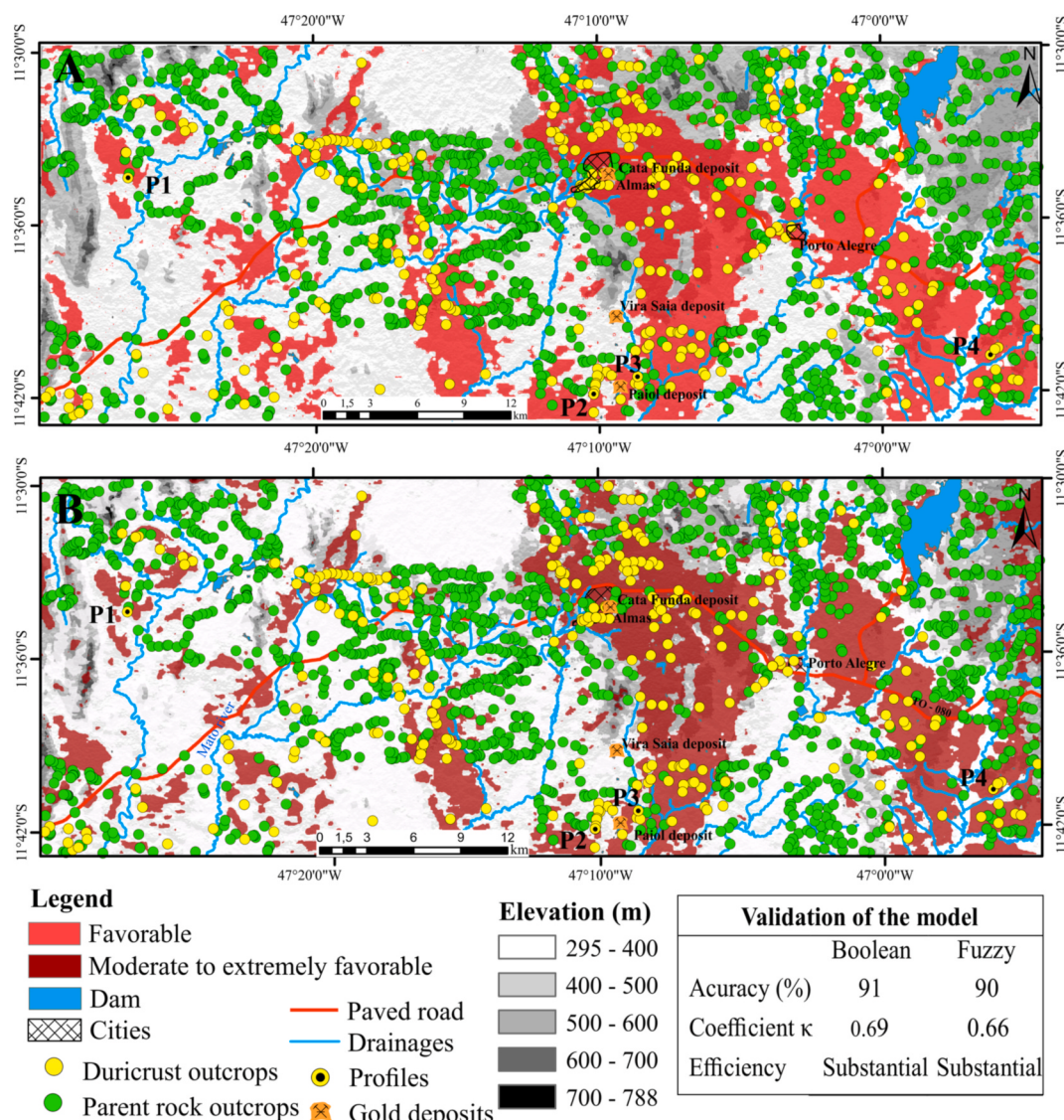


**Fig. 11.** Predictive maps of lateritic duricrust occurrence using Boolean (A) and fuzzy (B) logics (algorithm 4). Areas in red are lateritic duricrusts, mottled horizon, and soil, whereas the remaining area consists of parent rock and saprolite.

**Table 7**  
Pearson correlation coefficient ( $r$ ) results.

	WC	Elevation*	eTh	eU	K	$\frac{eTh + eU}{K}$
WC	1.00	<b>0.18</b>	<b>0.58</b>	<b>0.52</b>	-0.12	<b>0.76</b>
Elevation		1.00	0.31	0.23	0.49	-0.04
eTh			1.00	0.81	0.51	0.58
eU				1.00	0.41	0.53
K					1.00	-0.26
$eTh + eU$						1.00
$K$						

Note<sup>4</sup>. (1) WC = weathering class described in Table 2. SRTM\* = Shuttle Radar Topography Mission; (2) Bold values were referenced in the text.

**Table 8**  
Summary of stepwise regression.

Regression statistic	Coefficients	Standard error	Individual p-value
r multiple	0.790		
$r^2$	<b>0.624</b>		
$r^2$ adjusted	<b>0.623</b>		
Standard error	0.585		
Global p-value of F test	<b>0.000</b>		
Intersection	-1.2810	0.1366	$2.1332 \times 10^{-20}$
Elevation	0.0034	0.0003	$9.5602 \times 10^{-25}$
eTh	0.0310	0.0066	$5.5578 \times 10^{-11}$
$eTh + eU$	0.2327	0.0064	$3.3357 \times 10^{-218}$
$K$			

gamma-ray spectrometry to map the regolith in the midwestern part of the study site, where there is lateritic duricrust in small outcrops (less than 50 m in diameter) and therefore they are difficult to identify using the methods presented above (Fig. 7D, yellow dots in dark zones in the midwestern region). The choice of the optimal number of classes that represent the materials that make up the regolith strongly influences the quality of the predictive map, and must be adapted to the environmental context of the study region (Wilford, 2012; Iza et al., 2018). For the study region, tests showed that five classes for the WII map produced a

satisfactory result (accuracy 88%), as shown in Fig. 12.

Despite the possibility of gamma-ray attenuation by vegetation (Wilford, 1997), the manganese lateritic duricrust on gabbro (Serra do Boqueirão Suite) (Fig. 1, profile 4) in the dense vegetation covers in the southeastern part of the study region was highlighted by Boolean and fuzzy (FAPO) logics and WII. This was a consequence of the manganese duricrust having higher eTh (28.8 ppm) and eU (4.6 ppm) than the ferruginous lateritic duricrusts (8.9 and 2.4 ppm, respectively), which was validated by chemical analysis which showed higher concentrations of Th and U (12.7 and 4.1 ppm, respectively) in the manganese duricrust than in the ferruginous duricrust (6.8 and 2.1 ppm, respectively), as shown in Table 3. A recent study in southwestern Amazonia provided similar findings (Albuquerque et al., 2020). Thus, the gamma-ray spectrometry algorithms were found to be suitable also for mapping manganese lateritic duricrusts.

The misinformation about data input is an issue in the application of Boolean and fuzzy logic mapping techniques. When normalized data (256 Gy levels; K, eTh, eU, and their ratios) are used, the lateritic duricrust areas may be overestimated, as shown in algorithms 1, 2, and 3. The assigning of weights to the variables (IOM) instead of using the AND operator can provide better Boolean and fuzzy predictive maps. Considering that the airborne gamma-ray spectrometry data were acquired along a series of approximately parallel survey lines, and then it was interpolated using minimum curvature algorithm into a regular grid network, it is expected that noise, effects of data density and from the interpolation are smoothed (Dentith and Mudge, 2014). Therefore, it is necessary to test several combinations as well as input data formats validated by fieldwork and geological and geomorphological support to identify the most accurate results for a given region.

There are some limitations to the interpretation of gamma-ray spectrometry data associated with the algorithms and mapping techniques. The most obvious limitation is that regolith materials do not have unique gamma-ray signature, therefore gamma-ray data for regolith mapping is best used together with other datasets including multispectral, geochemistry, and altimetric data. Multispectral data can be used to create images showing the distribution of clays and iron oxides, both of which influence the distribution of K, Th and U (Dauth, 1997;

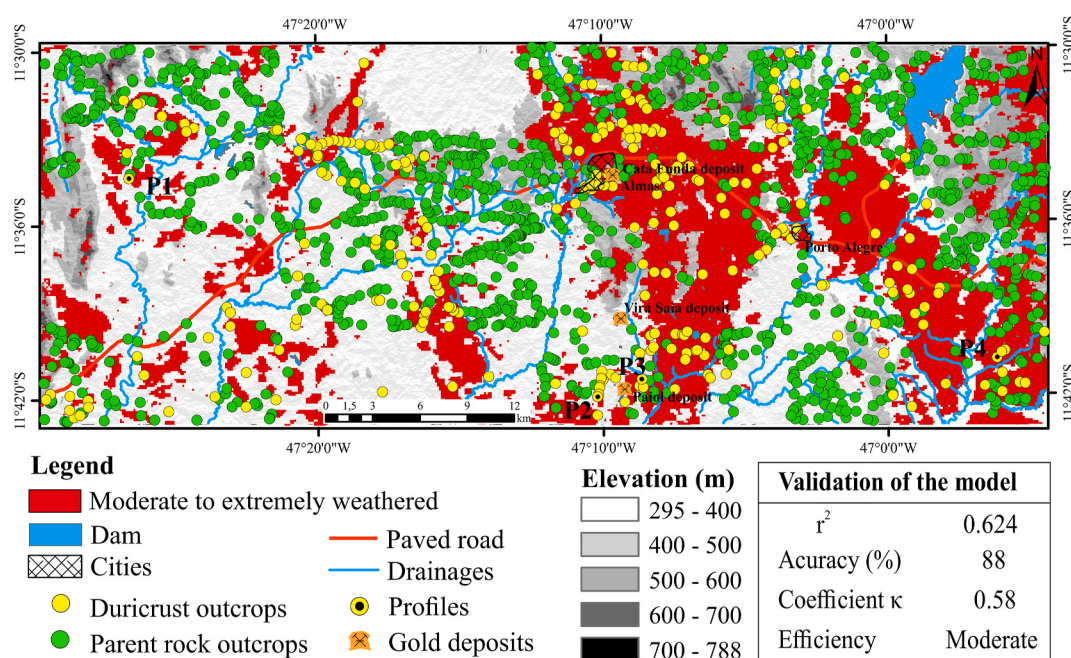


**Fig. 12.** The WII map overlaid on the shaded altimetry, highlighting moderate to intensely weathered areas (lateritic duricrusts, mottled horizon, and soil), as predicted by the WII equation, whereas the remaining areas represent unweathered to slightly weathered areas (parent rock and saprolite).

Metelka et al., 2018). The dense vegetation cover may limit the application of gamma-ray spectrometry. The optical remote sensing is routinely employed in regolith mapping (Souza et al., 2021), including band ratios and principal component analysis. These techniques enhance the response of clay minerals and suppress the effects of vegetation (Crósta and Moore, 1989). Another limitation of the described techniques is that airborne gamma-ray acquisition systems have relatively large “footprints”. This results in poor spatial resolution for local-scale applications (Wilford and Minty, 2007).

## 6. Conclusions

The efficiency of airborne gamma-ray spectrometry and elevation (SRTM image) in predicting residual lateritic duricrust areas, including mottled horizon and soil, relative to saprolite and parent rock outcrops in tropical terrains was highlighted using map algebra. The algorithm that used  $\frac{e\text{Th}+e\text{U}}{K}$  (in concentration) and elevation exported with appropriate extension to maintain the original data as airborne concentrations (algorithm 4) was the most efficient, with 91% accuracy, as compared to the other three algorithms (eTh in algorithm 1,  $\frac{e\text{Th}+e\text{U}}{K}$  in algorithm 2, and  $\frac{e\text{Th}+e\text{U}}{K}$  in algorithm 3, exported from GIS software as a compressed digital image data integrated with elevation using the Boolean and fuzzy operators).

The classification of WC, eTh, eU,  $\frac{e\text{Th}+e\text{U}}{K}$ , and elevation using Pearson correlation coefficient and multivariate linear regression for WII also yielded accurate predictive maps of regolith. Thus, integration of multisource data resulted in efficient mapping algorithms for the regolith in the study region. These algorithms help provide new guidelines and strategies for rapid selection of target sites for regolith exploration and have large applicability in regional geochemical interpretation and geological map reinterpretation.

The predictive mapping tools used in this study (e.g., weathering intensity index) allowed to discriminate areas in different degrees of weathering. The successful application of this technique for mapping regoliths is due to the effects of weathering, where radioelements contained in the rock are released, redistributed, and incorporated into the weathering products, modifying the gamma-spectrometric pattern of the underlying primary rocks. This approach is the key concept to design the algorithms used in this study.

## Credit author statement

Author 1: prepared the manuscript. Author 2: supervised all stages of preparing the manuscript. Participated in fieldwork, discussed the data, and revised the manuscript. Author 3: helped in the implementation of Boolean and fuzzy logics. Author 4: helped collect and prepare samples for mineral and chemical composition. Author 5: helped process airborne gamma-ray data. Author 6: contributed to the discussion of data and revision of the manuscript.

## Declaration of competing interest

The authors declare that they have no known competing financial interests or personal relationships that could have appeared to influence the work reported in this paper.

## Acknowledgments

The authors thank Serviço Geológico do Brasil - CPRM for providing the aerogeophysical data (<http://geosgb.cprm.gov.br/>), Universidade de Brasília and CAPES (Coordenação de Aperfeiçoamento de Pessoal de Nível Superior) for the technical and physical support, Instituto Natureza do Tocantins (NATURATINS/Governo do Estado do Tocantins) and Conselho Nacional de Desenvolvimento Científico e Tecnológico (CNPQ) for financial support (grant nº 302618/2016-3) and to the

reviewers and editor for their valuable criticisms and suggestions.

## References

- Albuquerque, M.F.S., Horbe, A.M.C., Soares, T.M., Sousa, E.M.D., Iza, E.R.H.F., 2020. Airborne radiometric data for identifying lateritic surface in southwestern Amazonia, Brazil. *J. Appl. Geophys.* 175, 103989. <https://doi.org/10.1016/j.jappgeo.2020.103989>.
- Anand, R.R., 2001. Evolution, classification and use of ferruginous materials in gold exploration, Yilgarn craton, Western Australia. *Geochem. Explor. Environ. Anal.* 1, 221–236. <https://doi.org/10.1144/geochem.1.3.221>.
- Anand, R.R., Butt, C.R.M., 2010. A guide for mineral exploration through the regolith in the Yilgarn Craton, western Australia. *Aust. J. Earth Sci.* 57, 1015–1114. <https://doi.org/10.1080/08120099.2010.522823>.
- Anand, R.R., Paine, M., 2002. Regolith geology of the yilgarn craton, western Australia: implications for exploration. *Aust. J. Earth Sci.* 49, 3–162. <https://doi.org/10.1046/j.1440-0952.2002.00912.x>.
- Arhin, E., Jenkin, G.R.T., Cunningham, D., Nude, P., 2015. Regolith mapping of deeply weathered terrain in savannah regions of the Birimian Lawra Greenstone Belt, Ghana. *J. Geochem. Explor.* 159, 194–207. <https://doi.org/10.1016/j.geexplo.2015.09.008>.
- Barbosa, I.O., Pires, A.C.B., Lacerda, M.P.C., Carmelo, A.C., 2013. Geology, airborne geophysics, geomorphology and soils in the individualization of the niquelândia mafic-ultramafic complex, Goiás state, Brazil. *Rev. Bras. Geofis.* 31, 463–481. <https://doi.org/10.22564/rbfg.v31i3.316>.
- Barnes, S.J., Fisher, L.A., Anand, R., Uemoto, T., 2014. Mapping bedrock lithologies through in situ regolith using retained element ratios: a case study from the Agnew-Lawlers area, Western Australia. *Aust. J. Earth Sci.* 61, 269–285. <https://doi.org/10.1080/08120099.2014.862302>.
- Bonham-Carter, G., 1994. *Geographic Information Systems for Geoscientists: Modelling with GIS*. Pergamon, Oxford.
- Borges, M., 1993. *Evolução tectono-estrutural da região de Dianópolis-Almas, SE do Estado do Tocantins*. Tese (doutorado em geologia). Universidade Federal do Pará, Belém, Brasil, p. 365p.
- Bowell, R.J., Afreh, E.O., Laffoley, N. d'A., Hanssen, E., Abe, S., Yao, R.K., Pohl, D., 1996. *Geochemical exploration for gold in tropical soils — four contrasting case studies from West Africa*. *Institution of Mining and Metallurgy Transactions* 105, B12–B33.
- Campos, D.S. de, Toledo, C.L.B., Carvalho, M.J. de, Rodrigues, V.G., Araujo, K., Silva, A. M., 2017. Prospectivity analysis of gold and iron oxide copper-gold-(silver) mineralizations from the Faina Greenstone Belt, Brazil, using multiple data sets. *Brazilian J. Geol.* 47, 561–590. <https://doi.org/10.1590/2317-4889201720170012>.
- Campos, J.E.G., et al., 2016. *Mapa base integrado. Projeto Almas 2016. Escala 1:50.000 [Trabalho final de graduação]*. Universidade de Brasília, Curso de Geologia, Instituto de Geociências.
- Carranza, E.J.M., 2011. *Geocomputation of mineral exploration targets*. *Comput. Geosci.* 37, 1907–1916.
- Carranza, E.J.M., Mangaoang, J.C., Hale, M., 1999. Application of mineral exploration models and GIS to generate mineral potential maps as input for optimum land-use planning in the Philippines. *Nat. Resour. Res.* 8, 165–173. <https://doi.org/10.1023/A:1021846820568>.
- Carrino, T.A., Silva, A.M., Botelho, N.F., da Silva, A.A.C., 2011. Discriminação de áreas de espesso regolito do leste do estado do Amazonas usando estatística multivariada, algoritmo hiperespectral e modelagem de dados espaciais. *Rev. Bras. Geofis.* 29, 155–172. <https://doi.org/10.1590/S0102-261X2011000100011>.
- Cohen, J., 1960. A coefficient of agreement for nominal scales. *Educ. Psychol. Meas.* 20, 37–46. <https://doi.org/10.1177/00131644600200104>.
- Cohen, J., 1988. *Statistical Power Analysis for the Behavioral Sciences*, second ed. Erlbaum, Hillsdale, NJ. <https://doi.org/10.4324/9780203771587>.
- Corrêa, R.S., Oliveira, C.G., Vidotti, R.M., Souza, V.S., 2015. Regional-scale pressure shadow-controlled mineralization in the príncipe orogenic gold deposit, Central Brazil. *Ore Geol. Rev.* 71, 273–304.
- Costa, J.B.S., 1985. Aspectos lito-estruturais e evolução crustal da região centro-oeste de Goiás. Universidade Federal do Pará.
- Costa, M.L., 1997. Lateritization as a major process of ore deposit formation in the amazon region. *Explor. Min. Geol.* 6, 79–104.
- CPRM - Serviço Geológico do Brasil, 2014. *Carta geológica. Projeto sudeste do Tocantins. Folha SC.23-Y-C - dianópolis*. In: Sabóia, A.M., Maneghini, P.F.V. (Eds.), Gonçalves, F.G. (org.). Escala 1:250.000.
- CPRM - Serviço Geológico do Brasil, 2006. Projeto Aerogeofísico do Tocantins, Relatório Final do Levantamento e processamento de dados magnetométricos e gamaespectrométricos. Available at: <http://geosgb.cprm.gov.br/>. (Accessed 25 November 2017).
- Craig, M.A., 2001. Regolith mapping for geochemical exploration in the Yilgarn craton, Western Australia. *Geochem. Explor. Environ. Anal.* 1, 383–390.
- Crósta, A.P., Moore, J.M., 1989. Enhancement of Landsat Thematic Mapper imagery for residual soil mapping in SW Minas Gerais state Brazil: a prospecting case history in Greenstone belt terrain. *Proc. 7th Them. Conf. Remote Sens. Explor. Geol. Calgary* 1173–1187.
- Cruz, E.L.C.C., Kuyumjian, R.M., 1998. Geology and tectonic evolution of the Tocantins granito-greenstone terrane: Almas-Dianópolis region, Tocantins State, central Brasil. *Rev. Bras. Geociências* 28, 173–182.
- Cruz, E.L.C.C., Kuyumjian, R.M., 1999. Mineralizações auríferas filoneanas do terreno granito-greenstone do Tocantins. *Rev. Bras. Geociências* 29, 291–298.

- Cruz, E.L.C.C., Kuyumjian, R.M., 2006. Geochronology, isotopic signature and metallogenetic model for the Córrego Paiol gold deposit, Tocantins state, central Brazil. *Rev. Bras. Geociencias* 36 (1-Suplemento), 152–156.
- Dauth, C., 1997. Airborne magnetic, radiometric and satellite imagery for regolith mapping in the Yilgarn Craton of Western Australia. *Explor. Geophys.* 28, 199–203. <https://doi.org/10.1071/EG997199>.
- Davy, R., El-Ansary, M., 1986. Geochemical Patterns in the laterite profile at the boddington gold deposit, western Australia. *J. Geochem. Explor.* 26, 119–144. [https://doi.org/10.1016/0375-6742\(86\)90062-2](https://doi.org/10.1016/0375-6742(86)90062-2).
- Dent, D.L., MacMillan, R.A., Mayr, T.L., Chapman, W.K., Berch, S.M., 2013. Use of airborne gamma radiometrics to infer soil properties for a forested area in British Columbia, Canada. *J. Ecosyst. Manag.* 14, 1–12.
- Denthith, M., Mudge, S., 2014. Geophysics for the Mineral Exploration Geoscientist. Cambridge University Press, Cambridge. <https://doi.org/10.1017/CBO9781139024358>.
- Dickson, B.L., Scott, K.M., 1997. Interpretation of aerial gamma-ray surveys—adding the geochemical factors. *J. Aust. Geol. Geophys.* 17, 187–200.
- Eddy, B.G., Graham, D.F., Bonham-Carter, G.F., Jefferson, C.W., 2006. Mineral potential analyzed and mapped at multiple scales—a modified fuzzy logic method using digital geology. In: Harris, J.R. (Ed.), *GIS for the Earth Sciences*. Geological Association of Canada, pp. 143–162.
- Freyssinet, Ph., Butt, C.R.M., Morris, R.C., Piantone, P., 2005. Ore-forming processes related to lateritic weathering. *Econ. Geol.* 100th Anniv. 1, 681–722.
- Freyssinet, Ph., Zeegers, H., Tardy, Y., 1989. Morphology and geochemistry of gold grains in lateritic profiles from South Mali. *J. Geochem. Explor.* 32, 99–116.
- Grimaud, J.L., Chardon, D., Metelka, V., Beauvais, A., Bamba, O., 2015. Neogene cratonic erosion fluxes and landform evolution processes from regional regolith mapping (Burkina Faso, West Africa). *Geomorphology* 241, 315–330. <https://doi.org/10.1016/j.geomorph.2015.04.006>.
- Horbe, A.M., Costa, M., 1999. Geochemical evolution of a lateritic Sn–Zr–Th–Nb–Y–REE-bearing ore body derived from apogranite: the case of Pitinga, Amazonas – Brazil. *J. Geochem. Explor.* 66, 339–351. [https://doi.org/10.1016/S0375-6742\(99\)00002-3](https://doi.org/10.1016/S0375-6742(99)00002-3).
- IAEA - International Atomic Energy Agency, 1991. *Airborne Gamma Ray Spectrometer Surveying*. Technical Reports Series N° 323. Viena.
- Iza, E.R.H. de, F., Horbe, A.M.C., Silva, A.M., 2016. Boolean and fuzzy methods for identifying lateritic regoliths in the Brazilian Amazon using gamma-ray spectrometric and topographic data. *Geoderma* 269, 27–38. <https://doi.org/10.1016/j.geoderma.2016.01.037>.
- Iza, E.R.H.F., Horbe, A.M.C., Castro, C.C., Herrera, I.L.I.E., 2018. Integration of geochemical and geophysical data to characterize and map lateritic regolith: an example in the Brazilian Amazon. *G-cubed* 19, 3254–3271. <https://doi.org/10.1029/2017GC007352>.
- Jayawardhana, P.M., Sheard, S.N., 2000. The use of airborne gamma-ray spectrometry—a case study from the Mount Isa inlier, northwest Queensland, Australia. *Geophysics* 65. <https://doi.org/10.1190/1.1444883>, 1993–2000.
- Jost, H., Chemale, F., Dussin, I.A., Tassanari, C.C.G., Martins, R., 2010. A U-Pb zircon Paleoproterozoic age for the metasedimentary host rocks and gold mineralization of the Crixás greenstone belt, Goiás, Central Brazil. *Ore Geol. Rev.* 37, 127–139. <https://doi.org/10.1016/j.oregeorev.2010.01.003>.
- Jost, H., Fortes, P.T.F.O., 2001. Gold deposits and occurrences of the Crixás goldfield, central Brazil. *Miner. Depos.* 36 (3–4), 358–376.
- Klir, G.J., 2004. Fuzzy logic: a specialized tutorial. In: Demicco, R.V., Klir, G.J. (Eds.), *Fuzzy Logic in Geology*. Elsevier Academic Press, San Diego, pp. 11–61.
- Kuyumjian, R.M., Cruz, E.L.C.C., Araújo Filho, J.O., Moura, M.A., Guimarães, E.M., Pereira, K.M.S., 2012. Geologia e ocorrências de ouro do Terreno Granito-Greenstone do Tocantins, TO: síntese do conhecimento e parâmetros para exploração mineral. *Rev. Bras. Geociencias* 42, 213–228. <https://doi.org/10.25249/0375-7536.2012421213228>.
- Landis, J.R., Koch, G.G., 1977. The measurement of observer agreement for categorical data. *Source: Biometrics* 33, 159–174.
- Larizzatti, J.H., Oliveira, S.M.B., Butt, C.R.M., 2008. Morphology and composition of gold in a lateritic profile, Fazenda Pison garimpo, Amazonas, Brasil. *J. South Am. Earth Sci.* 25, 359–376. <https://doi.org/10.1016/j.jsames.2007.06.002>.
- Lobato, L.M., Ribeiro-Rodrigues, L.C., Vieira, F.W.R., 2001. Brazil's premier gold province. Part 11: geology and genesis of gold deposits in the Archean rio das velhas greenstone belt. *Quadrilatero ferriero. Miner. Depos.* 36, 249–277. <https://doi.org/10.1007/s001260100180>.
- Martelet, G., Drufin, S., Tourliere, B., Saby, N.P.A., Perrin, J., Deparis, J., Prognon, F., Jolivet, C., Ratie, C., Arrouays, D., 2013. Regional regolith parameter prediction using the proxy of airborne gamma ray spectrometry. *Vadose Zone J.* 12 (4) <https://doi.org/10.2136/vzj2013.01.0003>.
- Martelet, G., Truffert, C., Tourliere, B., Ledru, P., Perrin, J., 2006. Classifying airborne radiometry data with Agglomerative Hierarchical Clustering: a tool for geological mapping in context of rainforest (French Guiana). *Int. J. Appl. Earth Obs. Geoinf.* 8, 208–223. <https://doi.org/10.1016/j.jag.2005.09.003>.
- Martins-Ferreira, M.A.C., Campos, J.E.G., Pires, A.C.B., 2017. Near-mine exploration via soil geochemistry multivariate analysis at the Almas gold province, Central Brazil: a study case. *J. Geochem. Explor.* 173, 52–63. <https://doi.org/10.1016/j.gexplo.2016.11.011>.
- Metelka, V., Baratoux, L., Jessell, M.W., Barth, A., Jezek, J., Naba, S., 2018. Automated regolith landform mapping using airborne geophysics and remote sensing data, Burkina Faso, West Africa. *Remote Sens. Environ.* 204, 964–978.
- Moonjun, R., Shrestha, D.P., Jettena, V.G., Ruitenbeek, F.A.J.V., 2017. Application of airborne gamma-ray imagery to assist soil survey: a case study from Thailand. *Geoderma* 289, 196–212. <https://doi.org/10.1016/j.geoderma.2016.10.035>.
- Nykänen, V., Groves, D.J., Ojala, V.J., Eliu, P., Gardoll, S.J., 2008. Reconnaissance-scale conceptual fuzzy-logic prospectivity modelling for iron oxide copper - gold deposits in the northern Fennoscandian shield, Finland. *Aust. J. Earth Sci.* 55, 25–38. <https://doi.org/10.1080/08120090701581372>.
- Oliveira, S.M.B., Campos, E.G., 1991. Gold-bearing iron duricrust in Central Brazil. *J. Geochem. Explor.* 41, 309–323. [https://doi.org/10.1016/0375-6742\(91\)90005-F](https://doi.org/10.1016/0375-6742(91)90005-F).
- Oliveira, C.G., Oliveira, F.B., Giustina, M.E.S.D., Marques, G.C., Dantas, E., Pimentel, M.M., Buhn, B.M., 2015. The Chapada Cu–Au deposit, Mara Rosa magmatic arc, Central Brazil: constraints on the metallogenesis of a Neoproterozoic large porphyry-type deposit. *Ore Geol. Rev.* 72, 1–21. <https://doi.org/10.1016/j.oregeorev.2015.06.021>.
- Oliveira, C.G., Pimentel, M.M., Melo, L.V., Fuck, R.A., 2004. The copper–gold and gold deposits of the Neoproterozoic Mara Rosa magmatic arc, central Brazil. *Ore Geol. Rev.* 25, 285–299. <https://doi.org/10.1016/j.oregeorev.2004.04.006>.
- O'Reilly, G.A., Corey, M.C., Ford, K.L., 1988. The role of airborne gamma-ray spectrometry in bedrock mapping and mineral exploration: case studies from granitic rocks within the Meguma Zone, Nova Scotia. *Marit. Sediments Atl. Geol.* 4, 47–60.
- Ormeling, F.J., Kraak, M.J., 2008. Maps as predictive tools – mind the gap. *Cartographica* 43, 125–130.
- Pimentel, M.M., Fuck, R.A., Jost, H., Ferreira Filho, C.F., Araújo, S.M., 2000. The basement of the Brasília fold belt and the Goiás magmatic arc. In: Cordani, U.G., Milani, E.J., Thomaz Filho, A., Campos, D.A. (Eds.), *Tectonic Evolution of South America*. Rio de Janeiro: 31st IGC. 190–229.
- Pires, A.C.B., 1995. Identificação geofísica de áreas de alteração hidrotermal, Crixás-Guarinos. *Rev. Bras. Geoc.* 25 (1), 61–68. <https://doi.org/10.25249/0375-7536.19956168>.
- Porto, C.G., Hale, M., 1996. Mineralogy, morphology and chemistry of gold in the stone line lateritium profile of the Posse deposit, Central Brazil. *J. Geochem. Explor.* 57, 115–125. [https://doi.org/10.1016/S0375-6742\(96\)00027-1](https://doi.org/10.1016/S0375-6742(96)00027-1).
- Porwal, A., Deb Das, R., Chaudhary, B., Gonzalez-Alvarez, I., Kreuzer, O., 2015. Fuzzy inference systems for prospectivity modeling of mineral systems and a case-study for prospectivity mapping of surficial Uranium in Yeelirrie Area, Western Australia. *Ore Geol. Rev.* 71, 839–852. <https://doi.org/10.1016/j.oregeorev.2014.10.016>.
- Raines, G.L., Sawatzky, D.L., Bonham-Carter, G.F., 2010. New Fuzzy Logic Tools in ArcGis 10. ArcUser, ESRI.
- Santosh, M., Omana, P.K., Yoshida, M., 1990. Gold grains in laterite weathering profiles of Nilambur, South India and a model for the genesis of supergene gold deposits. *Journal of Mineralogy Petrography and Economic Geology* 85, 416–423.
- SEPLAN - Secretaria do Planejamento e da Modernização Pública, 2012. *Atlas do Tocantins: Subsídios ao Planejamento da Gestão Territorial, Superintendência de Pesquisa e Zoneamento Ecológico-Econômico. Diretoria de Zoneamento Ecológico-Econômico – DZE, Palmas*.
- Silva, A.M., Pires, A.C.B., MacCafferty, A., Moraes, R.A.V. de, Xia, H., 2003. Application of airborne geophysical data to mineral exploration in the uneven exposed terrains of the Rio das Velhas Greenstone Belt. *Rev. Bras. Geociencias* 33 (2-Suplemento), 17–28.
- Smith, R.E., Anand, R.R., Alley, N.F., 2000. Use and implications of paleoweathering surfaces in mineral exploration in Australia. *Ore Geol. Rev.* 16, 185–204. [https://doi.org/10.1016/S0169-1368\(99\)00030-X](https://doi.org/10.1016/S0169-1368(99)00030-X).
- Souza, M.V., Horbe, A.M.C., Silva, B.C., Peixoto, S.F., Castro, R.T., 2021. Regolith LANDSAT-8/OLI and hyperion/EO-1 images classification in midwest of Brazil. *J. S. Am. Earth Sci.* 111, 103460. <https://doi.org/10.1016/j.jsames.2021.103460>.
- Tomlin, C.D., 1994. Map algebra: one perspective. *Landscape Urban Plann.* 30, 3–12.
- Viera, A.J., Garrett, J.M., 2005. Understanding interobserver agreement: the kappa statistic. *Fam. Med.* 37 (5), 360–363.
- Voll, E., Silva, A.M., Pedrosa-Soares, A.C., 2020. Tracking iron-rich rocks beneath Cenozoic tablelands: an integration of geological, airborne geophysical and remote sensing data from northern Minas Gerais State, SE Brazil. *J. South Am. Earth Sci.* 101, 102604. <https://doi.org/10.1016/j.jsames.2020.102604>.
- Wilford, J.R., 1995. Airborne gamma-ray spectrometry as a tool for assessing relative landscape activity and weathering development of regolith, including soils. *Australian Geological Survey Organisation Research Newsletter* 22, 12–14.
- Wilford, J.R., 2012. A weathering intensity index for the Australian continent using airborne gamma-ray spectrometry and digital terrain analysis. *Geoderma* 183–184, 124–142. <https://doi.org/10.1016/j.geoderma.2010.12.022>.
- Wilford, J.R., Bierwirth, P.N., Craig, M.A., 1997. Application of airborne gamma-ray spectrometry in soil/regolith mapping and applied geomorphology. *AGSO J. Aust. Geol. Geophys.* 17 (2), 201–216.
- Wilford, J., Minty, B., 2007. The use of airborne gamma-ray imagery for mapping soils and understanding landscape processes. In: Lagacherie, P., McBratney, A.B., Voltz, M. (Eds.), *Digital Soil Mapping an Introductory Perspective*. Developments in Soil Science, vol. 31. Elsevier.
- WRB, 2015. *World Reference Base for Soil Resources 2014, Update 2015. International Soil Classification System for Naming Soils and Creating Legends for Soil Maps*. World Soil Resources Reports No. 106. FAO, Rome.
- Yang, Y., Liu, S., Jin, Z., 2009. Laterization and its control to gold occurrence in Laowanchang gold deposit, Guizhou Province, Southwest of China. *J. Geochem. Explor.* 100, 67–74. <https://doi.org/10.1016/j.gexplo.2008.04.004>.
- Zadeh, L.A., 1965. Fuzzy sets. *Inf. Contr.* 8 (3), 338–353.
- Zimmermann, H.J., 1985. *Fuzzy Set Theory—And its Applications*. Kluwer Academic Publishers, Dordrecht.